# PhaseMO: A Universal Massive MIMO Architecture for Sustainable NextG

Adel Heidari, Agrim Gupta, Ish Kumar Jain, and Dinesh Bharadia University of California, San Diego, USA {adheidari, agg003, ikjain, dbharadia}@ucsd.edu

Abstract—The rapid proliferation of devices and increasing data traffic in cellular networks necessitate advanced solutions to meet these escalating demands. Massive MIMO (Multiple Input Multiple Output) technology offers a promising approach, significantly enhancing throughput, coverage, and spatial multiplexing. Despite its advantages, Massive MIMO systems often lack flexible software controls over hardware, limiting their ability to optimize operational expenditure (OpEx) by reducing power consumption while maintaining performance. Current software-controlled methods, such as antenna muting combined with digital beamforming and hybrid beamforming, have notable limitations. Antenna muting struggles to maintain throughput and coverage, while hybrid beamforming faces hardware constraints that restrict scalability and future-proofing. This work presents PhaseMO, a versatile approach that adapts to varying network loads. PhaseMO effectively reduces power consumption in low-load scenarios without sacrificing coverage and overcomes the hardware limitations of hybrid beamforming, offering a scalable and future-proof solution. We will show that PhaseMO can achieve up to 30% improvement in energy efficiency while avoiding about 10% coverage reduction and a 5dB increase in UE transmit power.

Index Terms—Universal Beamforming, massive MIMO, Sustainable NextG, Spatial Multiplexing, Digital Beamforming, Hybrid Beamforming

## I. INTRODUCTION

With every cellular generation, the number of antennas increases, since more antennas allow access to spatial degrees of freedom. This provides benefits like increased coverage, higher throughput, and spatial multiplexing to help scale to a large number of users and exponential growth in mobile networks. At present, the most deployed multi-antenna technology is Massive MIMO, which utilizes a 'massive' number of antennas, that can be as high as 64-128, to provide increased coverage >1 km, net throughputs over 1 Gbps, and the ability to multiplex 8-16 users in the spatial domain [1].

For considering the ease of deployment, most often these performance metrics (throughput, coverage) are reported when the Massive MIMO array is being fully utilized, and considered as the peak performance. As cellular networks mature and evolve into the next generation, softwarized control over the radio hardware has emerged as an important theme [2]. Softwarized control provides greater flexibility over the hardware [3], and reduction of operational expenditure (OpEx) by tuning down the power consumption when network conditions don't require peak performance [4]. In the context of Massive MIMO, such softwarized control aims to judiciously use the massive spatial degrees of freedom to optimize for the existing

network load conditions. For example, a Massive MIMO base station can reduce the number of spatially multiplexed layers under low load conditions, like night-time, and, hence save power. Further, this performance toning down should be flexible, and if needed, the underlying hardware needs to start working at the peak performance once the network load increases.

To make massive MIMO adapt to network load conditions, there are mainly two broad approaches studied in the literature: (1) Antenna muting-assisted Digital Beamformers [5] and (2) Hybrid Beamformers [6]. The majority of the existing Massive MIMO deployments utilize Digital Beamforming architecture, which has a separate digital RF chain interface for each antenna. Antenna muting approaches consist of softwarized control atop Digital Beamformers, which turn off a certain number of RF chains when the network load is low. Antenna muting adjusts the number of antennas as the network load varies, to improve energy efficiency by not using more than the required number of antennas. However, this leads to reduced user-perceived throughput, as well as increased userequipment power, since the overall antenna gain reduces due to muting, and this has been reported across multiple companies in the latest 3GPP reports [7]. The second solution, Hybrid Beamforming (HBF) aims to always utilize a large number of antennas while connecting them to a smaller number of RF chains via an analog network typically consisting of phase shifters. Since HBF doesn't reduce the number of antennas, but only the number of RF chains, it doesn't have the required drastic effect on throughput and user device power. However, HBF architectures are not flexible, and future-proof, that is, say we have an HBF that connects 64 antennas to 8 RF chains, it can not be scaled up to utilize the same hardware for 16 spatial multiplexed layers. That is, HBF architectures can only be designed for a particular network load, and are unable to scale up if needed in the future, which limits their real-world deployment.

In this work, we present PhaseMO, which enables the best elements from the prior two solutions, that is, flexible reduction of power, adaptive to network load, akin to antenna muting, and as well having the ability to use the entire antenna array like the hybrid beamformer, while reducing the RF chains. That is, in PhaseMO, the total digital compute can be optimized using software control to reduce the total number of RF chains, while always being connected to all the antennas using the proposed analog network architecture. Hence, PhaseMO maximally utilizes all the antennas' spatial

Beamforming	Data Streams	Energy Efficiency	Adaptability Future-Proof
Digital	Multiple	Low	No
Digital + AM	Multiple	Medium	Yes
Hybrid	Multiple	High	No
	(Restricted)		
PhaseMO	Multiple	High	Yes
	(Unrestricted)		

**TABLE I:** Comparison of beamforming techniques for spatial multiplexing: PhaseMO achieves higher energy efficiency and adaptive data stream scaling compared to DBF, AM-assisted DBF, and Hybrid Beamforming.

degrees of freedom to avail the maximum beamforming gain while reducing the digital processing power demanded by RF chains. This allows PhaseMO to operate at higher energy efficiencies than the existing solutions without creating any adverse effects on throughput, coverage, and user device power consumption. A summary of PhaseMO's provided features in comparison to existing approaches is shown in Table I.

To achieve high performance with reduced hardware complexity and scalability features, PhaseMO introduces a novel MIMO architecture that combines a single RF chain utilizing a high-sampling ADC/DAC and a network of Fast Phase Shifters (FPSs) which are replacing the traditional phase shifters and can provide phase shifts at sub-nanosecond speeds (faster than 1 GHz). These FPSs which are commercially available [8] enable the creation of V flexible "virtual" RF chains within a period of a single symbol. For example, with  $B=100~\mathrm{MHz}$ (symbol time = 10 ns) and V = 10, the FPSs update phase settings every 1 ns synchronous to ADC/DAC operating at VB net digital conversion rate, thus creating 10 different analog beam configurations within the net 10 ns time. This process essentially creates V = 10 different beam signals within a symbol time hence making PhaseMO, a future-proof architecture as it allows software control to scale the number of virtual RF chains V, by simply increasing the ADC/DAC sampling rate by V times and running the FPSs V times faster, without needing any hardware upgrades.

In this paper, we describe the required mathematical models to show the exact process behind the construction of these VRF chains, the required approximations, analog non-idealities, and their overall impact on the system performance. We show that by always utilizing the large number of antennas, PhaseMO performance matches throughput and coverage metrics of state-of-art hybrid beamformers, while capable of tuning up and down as needed. That is when V=1, PhaseMO takes the form of an analog beamformer, and when V = Nit becomes like a digital beamformer, while any intermediary value PhaseMO emulates a hybrid beamformer. Overall, this ability to control the digital compute based on the choice of V makes PhaseMO energy efficient, able to reduce power consumption while not introducing any detriments towards throughput, coverage, and user device power. The paper is organized as follows: Section II reviews related work, Section III outlines the system model, Section IV details the PhaseMO architecture, Section V evaluates PhaseMO's performance, and Section VI discusses its limitations and implications.

## II. RELATED WORK

Improving the energy efficiency of wireless networks is gaining interest from both academic research [9], [10], as well as industry standards having work items on network energy savings [7]. Researchers are actively exploring methods and techniques to reduce energy consumption by judicious use of the temporal [11], [12], frequency [13], [14], and spatial resources [15], [16] available to a radio.

In the context of Massive MIMO, the optimization of spatial resources is of primary importance. Here, antenna muting has emerged as an important method of reducing energy consumption, by optimizing the number of active antennas and hence the associated RF chains [5], [17], [18]. However, since antenna muting reduces the number of active antennas, it also causes adverse effects on throughput and coverage, as reported by multiple companies in the network energy study by 3GPP [7]. Further, to reduce this adverse impact, the required antenna selection algorithms to determine which antennas to mute are not straightforward. These algorithms often involve a data-driven approach to model the network load and fine-tune the algorithms properly to ensure that antenna muting adverse effects are reduced [19]–[21].

In comparison, there are alternate sets of works, that utilize all the antennas, but reduce the number of RF chains instead, by using Hybrid beamforming (HBF) approaches [6], [22]. Fully-connected HBF capture maximum array gain per RF chain [23], [24], unlike the partially connected HBF [25], [26] counterparts, which only have a subset of antennas connected. Hence, Fully-connected HBF increases energy efficiency by reducing the digital processing required [27], [28]. However, Fully-connected HBF is shown to have challenges in hardware implementations since they require complex analog networks with multiple splitter networks [29], [30], to ensure all the antennas are available to all the RF chains.

In addition to HBF, there are other proposed antenna arrays, that utilize RF switches [31]–[33] to multiplex multiple antennas via a single RF chain using time domain codes. Most notable of these is GreenMO [31], which implements such switched arrays for wideband OFDM waveforms and shows the feasibility of multiple antennas sharing a single RF chain to achieve energy efficiency. However, commercially available RF switches can only reach switching speeds of  $\sim 10 \, \rm ns$ , which limits the number of antennas that can share the same RF chain. This limits the scalability of these ideas. Further, RF switches only allow for antenna-selection-based beamforming gains, which fail to capture the maximum beamforming gains possible from co-phased combining across antennas.

In this paper, we show how using commercially available Fast Phase Shifters (FPS) [8] can effectively lead to both, faster multiplexing to increase the number of multiplexed antennas, as well as efficient co-phased combining across antennas to achieve full beamforming gain. They typically have voltage-controlled circuits that allow for high-speed phase changes in the order of 1 ns (symbol-level) at the cost of a little bit higher power consumption, quite faster than digital-controlled phase shifters [34] which usually work at the speed of slot time.

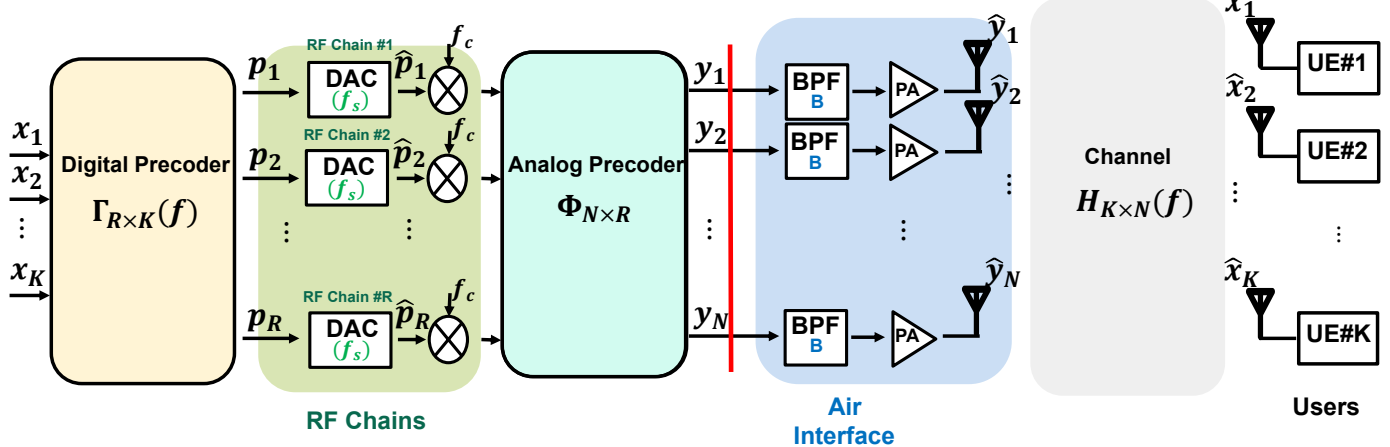


Fig. 1: A generic architecture model for beamforming structures, encompassing four parts: 1) Baseband Digital Precoder: Digital precoding over subcarriers on users' data vector  $X_{K\times 1}(f)$  with bandwidth B. 2) RF Chains: Precoded digital samples  $P_{R\times 1}(f)$  pass through DACs (sampling frequency  $f_s$ ) and upconverters to passband  $f_c$ , resulting in analog output signals  $\hat{P}_{R\times 1}(f)$ . 3) RF Analog Beamformer: Phase shifters perform analog precoding, mapping R RF chains' analog signals to R0 signals R1 interface Part: Power amplifiers, antennas, and bandpass filters operate on R2 to produce R3 to produce R4 with bandwidth R5 centered around R5.

#### III. SYSTEM MODEL

To analyze various beamforming architectures and their performance, we use a generic model encompassing all existing structures, as shown in Fig. 1. We illustrate how hardware architectural differences affect the mathematical model and performance. Using this model, we derive the signal expressions emitted from the antennas after digital and analog precoding. DAC non-idealities are excluded at this stage, assuming they are mitigated by the BPF in the air interface.

Consider a downlink scenario with N antennas and K users. The emitted signal is:

$$\hat{Y}_{N\times 1}(f) = \Phi_{N\times R} \Gamma_{R\times K}(f) X_{K\times 1}(f), \tag{1}$$

where  $\Phi_{N \times R}$  is the analog precoding matrix for N antennas and R physical RF chains,  $\Gamma_{R \times K}(f)$  is the digital precoding matrix, and  $X_{K \times 1}$  is the data for K user streams.

- Baseband Digital Precoder: The precoding matrix  $\Gamma_{R\times K}(f)$  applies baseband digital precoding across subcarriers to the users' data vector  $X_{K\times 1}(f)$ , which has a bandwidth B. This process generates R precoded signals,  $P_{R\times 1}=\Gamma_{R\times K}(f)X_{K\times 1}(f)$  each corresponding to an RF chain.
- RF Chains: The precoded digital samples are processed through RF chains, each comprising a digital-to-analog converter (DAC) with a sampling frequency  $f_s$  and an upconverter that shifts the baseband signal to the passband at  $f_c$ . The resulting analog signals,  $\hat{P}_{R\times 1} = A(\Gamma_{R\times K}(f)X_{K\times 1}(f))$ , include DAC non-idealities, such as sideband images near harmonics of the sampling frequency which is assumed this effect is modeled with the function A.

In other words, although the DAC's effect varies depending on the technology used in its operation, it is generally observed that the DAC output creates sideband spectrums of the main signal at sampling frequency products, with a sinc roll-off factor. For instance, if the DAC operates at a sampling frequency  $f_s$  on a signal with bandwidth B, it

will generate sidebands at multiples of  $f_s$ , each sideband having a bandwidth of B.

- RF Analog Beamformer: This involves a network of phase shifters that perform analog precoding on the passband signal. The analog precoding matrix,  $\Phi_{N\times R}$ , consisting of unity magnitude components with varying phases, maps the R RF chains' analog signals to N signals, denoted as  $Y_{N\times 1} = \Phi_{N\times R} A(\Gamma_{R\times K}(f) X_{K\times 1}(f))$ , which are then radiated by the antennas.
- Air Interface Part: This part comprises power amplifiers (PAs), antennas, and bandpass filters (BPFs). The BPF, placed before the PA, removes non-idealities from the DAC, upconverter, and other sources. With a bandwidth of B centered at  $f_c$ , it processes  $Y_{N\times 1}$  to produce  $\hat{Y}_{N\times 1}$ . Using BPF, we can assume the non-idealities sourced from the DAC shown with function A can be eliminated. Therefore, the emitted signal can be written as 1. It's worth noting that the setup for the air interface part is consistent for all the beamforming techniques.

Finally, we can write the received signals on the user side by considering the channel effect on the emitted signals.

$$\hat{X}_{K\times 1}(f) = H_{K\times N}(f)\Phi_{N\times R}\Gamma_{R\times K}(f)X_{K\times 1}(f)$$
 (2)

where  $H_{K\times N}(f)$  is the wireless channel between N antennas and K users. In the following subsections, we will discuss how different parts differ with respect to different beamforming techniques and how these differences affect the mathematical model and performance for each of them.

## 1) Digital beamforming

In a digital beamforming architecture, all precoding is performed on the digital symbols, eliminating the need for an analog precoder. As a result, the number of RF chains must equal the number of antennas, implying R=N. Consequently, the analog precoding matrix  $\Phi_{N\times R}$  reduces to the identity matrix  $I_{N\times N}$ , and the digital precoding matrix  $\Gamma_{R\times K}$  becomes  $\Gamma_{N\times K}$ . Therefore, the mathematical expression for the signals

emitted from the antennas in digital beamforming can be rewritten using Eq. 1 as  $\hat{Y}_{N\times 1}(f) = \Gamma_{N\times K}(f)X_{K\times 1}(f)$ .

## 2) Analog beamforming

Analog beamformers, which are structurally different from digital beamformers, do not utilize any digital precoder. Instead, a single RF chain is employed to convert digital symbols into an analog signal, limiting the architecture to support only one user's data transmission at a time  $(R = K = 1, X_{K\times 1}(f) = X_{1\times 1}(f), \text{ and } \Gamma_{1\times 1} = 1)$  which significantly reduces the system's throughput. In the analog domain, a network of phase shifters is used for precoding. This network comprises as many phase shifters as there are antennas (N) in the architecture, resulting in the analog precoder matrix being an  $N\times 1$  vector. However, the precoding performance is limited since the analog precoding matrix,  $\Phi_{N\times 1}$ , is not frequency-dependent, reducing its effectiveness for wideband systems. Thus, the analog beamformer expression can be rewritten using Eq. (1) as  $\hat{Y}_{N\times 1}(f) = \Phi_{N\times 1}X_{1\times 1}(f)$ .

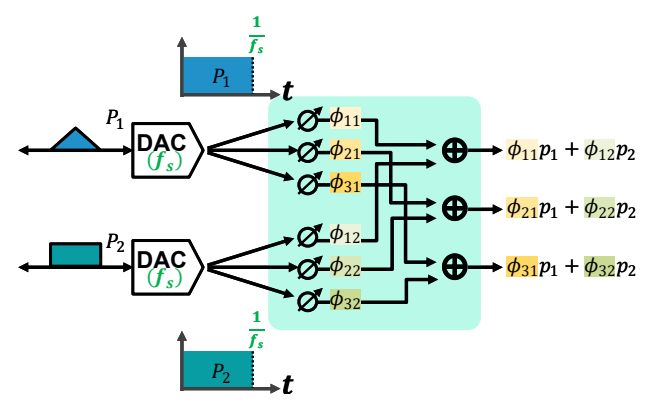
## 3) Hybrid beamforming

Hybrid beamforming combines a digital precoder and an analog beamformer, and its structure is accurately represented by the generic model in Fig. 1. This architecture features R RF chains that convert digitally precoded symbols,  $\Gamma_{R\times K}(f)$ , into analog signals, which are then beamformed via a phase shifter network and radiated from N antennas. The analog network can be fully connected, in which all R RF chains connect to all N antennas, or partially connected, in which each RF chain connects to a subset of antennas. Importantly, the maximum number of users supported is limited by the number of RF chains, R, and the analog precoder  $\Phi_{N\times R}$ , not being frequency-dependent, reduces performance in wideband systems. The mathematical representation of hybrid beamforming is given as  $Y_{N\times 1}(f) = \Phi_{N\times R}\Gamma_{R\times K}(f)X_{K\times 1}(f)$ , where  $\Phi_{N\times R}$  has sparse non-zero elements in partially connected architectures.

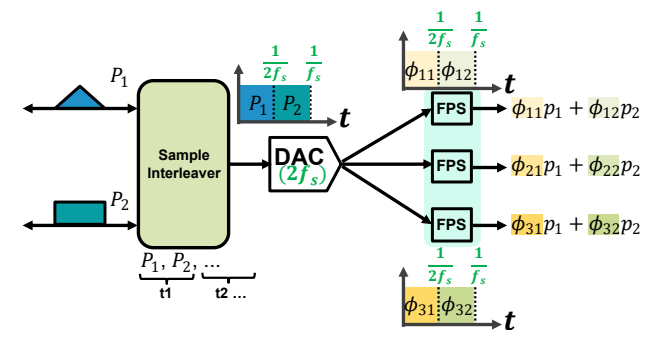
Next, we demonstrate the PhaseMO architecture, showcasing it as a viable alternative to all beamforming techniques with hardware complexity comparable to analog beamforming.

### IV. PHASEMO DESIGN

PhaseMO designs a new beamforming architecture that enables high coverage area and high throughput with a single RF chain that can adapt itself to network throughput demand. In this section, we first discuss how PhaseMO mimics the RF analog beamformer of traditional hybrid precoding through a simpler novel analog architecture using only a single RF chain to create N antenna signals in the time domain. Also, we will explain how PhaseMO gains softwarized control over the radio hardware to achieve flexible throughput beating hybrid beamforming hardware limitations. Next, we will present the combining method PhaseMO used to convert V digitally precoded signals of virtual RF chains into a single physical RF chain and demonstrate how it can be represented in the frequency domain for further explanation of the mathematical representation of the design. Finally, we will demonstrate



#### (a) Traditional Fully-Connected Hybrid-MIMO Architecture



#### (b) PhaseMO MIMO Architecture

Fig. 2: Traditional and PhaseMO beamforming architectures: a) Traditional beamforming architecture utilizes multiple RF chains, each corresponding to a precoded signal, followed by time-invariant phase shifters at each antenna. b) PhaseMO architecture combines all precoded signals into one via a digital interleaver, then passes it through a DAC operating at a higher frequency. Fast phase shifters at each antenna beamform the combined analog signal

the mathematical foundation of end-to-end communication via PhaseMO and illustrate how it has the potential to support different throughput ranges from digital beamforming to analog beamforming.

#### A. Beating hybrid beamforming's hardwarized flexibility

To practically realize how PhaseMO can generate multiple signals right after the single RF chain, and how it mimics the analog beamformer part of a traditional hybrid precoder, we consider Fig. 2. As shown in this figure, a case of three antennas with two digitally precoded signals is considered. 2.a) shows how traditional beamforming architecture utilizes two RF chains each of which with  $f_s$  sampling frequency and a 3 network of phase-shifters (PSs) to create three signals for radiation from the antennas. In this figure, we can see each RF chain is connected to all three antennas, and the signals that get radiated from the antennas are the summation of two phase-shifted RF chain signals which are produced via  $3 \times 2 = 6$  time-invariant PSs.

On the other hand, as shown in Fig. 2.b), PhaseMO uses only a single RF chain with two times more sampling frequency to convert digitally interleaved signals into a single analog signal which goes into 3 FPSs each of which has individual phase control and works at DAC sampling frequency of  $2f_s$ . In other words, the first FPS keeps changing its phase within  $\phi_{11}$  and  $\phi_{12}$  periodically and holds each phase for  $\frac{1}{2f_s}$ . As shown in Fig. 2, by configuring the FPSs to shift the phase

of signals in a specific pattern, we can exactly create the same signal produced in Fig. 2.a).

Furthermore, we can see if we had more digitally precoded signals (demand for more throughput), we could easily combine them to pass through the single physical RF chain with an increased sampling frequency proportionate to the number of precoded signals (Fig. 2.b). However, we need to increase the number of physical RF chains in traditional hybrid beamforming architecture to be able to achieve more degrees of freedom on digital beamforming or multiplexing more beams.

## B. PhaseMO's ability to mimic any traditional beamformer

Now, we can generalize the toy example discussed in Fig. 2.b) to unify the mathematical representation of the PhaseMO architecture, and show how PhaseMO can be configured to achieve any of the traditional beamforming schemes, explained in section III and shown with the mathematical representation of Eq. 1. A major assumption here is that the DAC's non-idealities combined with FPS spectrum spreading effects can be eliminated using the bandpass filter after the FPS perantenna, which will be detailed once we present the mathematical generalization.

As shown in Fig. 3, we consider N antennas, Kusers, and V virtual RF chains. If we denote V <=N as the number of digitally precoded symbols, we can combine all V precoded signals into a single stream using a sample interleaver. So, we can write the time domain interpretation of the interleaved signal as  $z[n] = [p_1[1], p_2[1], \dots, p_V[1], p_1[2], p_2[2], \dots, p_V[2], \dots]$ which  $p_v[m]$  denotes the m-th sample of the v-th digitally precoded time-domain vector (virtual RF chain). In other words, all the V vectors are upsampled by V and each of them is delayed by 0, 1, 2, ..., V symbols respectively. Once this signal goes to the DAC, each element in the vector will occupy  $\frac{1}{Vf_s}$  time duration, so a single element delay in the vector will act as  $\frac{1}{Vf_s}$  time delay. Since we want to analyze the signal's spectrum, we must write down the frequency domain representation of sample interleaver output in the analog domain ignoring the DAC's impacts as follows:

$$Z(f) = P_1(f) + e^{-\frac{j2\pi f}{Vf_s}} P_2(f) + \dots + e^{-\frac{j(V-1)2\pi f}{Vf_s}} P_V(f)$$
 (3)

Which  $e^{-\frac{jv2\pi f}{Vf_s}}$  represents the frequency-domain phase shift due to the time-domain delay for the vector of precoded symbols v -th. Notably, the effect of V-times upsampling is compensated by increasing the DAC sampling frequency by V-times.

In the next step, we consider the effect of FPS on the DAC output. As mentioned previously, each FPS toggles periodically between V phases each of which with  $\frac{1}{Vf_s}$  duration, for instance, FPS located at nth antenna creates  $\Phi_{n1}, \Phi_{n2}, ...$ , and  $\Phi_{nV}$  with period of  $\frac{1}{f_s}$ . Therefore, the radiated signal from the nth antenna can be determined as follows, which is the multiplication of constant periodic phases and DAC's output:

$$\hat{Y}_n(f) = \sum_{v=0}^{V-1} e^{j\Phi_{nv}} \left( P_1(f) + e^{-\frac{j2\pi f}{Vf_s}} P_2(f) + \dots + e^{-\frac{j(V-1)2\pi f}{Vf_s}} P_V(f) \right)$$
(4)

By considering  $\hat{P}_v(f) = P_v(f) e^{\frac{jv2\pi f}{Vfs}}$ , we can express the summation in the matrix form of  $\hat{Y}_{N\times 1}(f) = \Phi_{N\times V}\hat{P}_{V\times 1}(f)$ , which  $\Phi_{N\times V}$  represents the phase matrix represented by N FPSs. Furthermore, we can also include a digital precoding matrix denoted by  $\Gamma_{V\times K}(f)$  in this part to clarify the final radiated signal  $(\hat{P}_{V\times 1} = \Gamma_{V\times K}(f)X_{K\times 1}(f))$ :

$$\hat{Y}_{N\times 1}(f) = \Phi_{N\times V} \Gamma_{V\times K}(f) \mathbf{X}_{K\times 1}(f)$$
 (5)

We now aim to further explain the equation derived for the signal emitted from the antennas (Eq. 5) and discuss how PhaseMO can relate to the other beamforming techniques mentioned earlier.

- For V=N, the final equation can be written as  $\hat{Y}_{N\times 1}(f) = \Phi_{N\times N}\Gamma_{N\times K}(f)\mathbf{X}_{K\times 1}(f)$ . This equation is exactly similar to what we already derived for a digital beamformer if we consider  $\Phi_{N\times N}$  as an identity matrix which can be achieved using
- For **V=1**, the final equation can be written as  $\hat{Y}_{N\times 1}(f) = \Phi_{N\times 1}\mathbf{X}_{1\times 1}(f)$ . We can observe that this equation is in the same form as that for an analog beamformer, which uses just one RF chain. This shows that PhaseMO with V=1 can model an analog beamformer.
- For V=R, we consider V as the number of physical RF chains of the hybrid beamforming architecture, thus the final equation can be written as  $\hat{Y}_{N\times 1}(f) = \Phi_{N\times R}\Gamma_{R\times K}(f)\mathbf{X}_{K\times 1}(f)$ . This equation aligns with the form we have for a hybrid beamformer. It shows that PhaseMO with V=R can model a hybrid beamformer.

Notably, if we consider the channel, we can figure out what signal will be received on the user side:

$$\hat{X}_{K\times 1} = H_{K\times N}(f)\Phi_{N\times V}\Gamma_{V\times K}(f)\mathbf{X}_{K\times 1}(f) \tag{6}$$

Although the mathematical description assumes PhaseMO in a downlink scenario, by considering an ADC instead of a DAC and performing the desired interleaving, similar expressions can be derived for an uplink scenario as well. In conclusion, PhaseMO, with just a single RF chain, can adapt itself to different network throughputs in a softwarized manner.

# C. Eliminating DAC non-idealities and FPS spreading effect

So far, we have shown the design of the PhaseMO and explained how using the fast phase changes can provide an adaptive MIMO architecture under the assumption that the spreading effect and DAC non-idealities can be ignored using a bandpass filter. Here, we demonstrate the effect of the DAC on the signal's spectrum, which represents a major issue that needs to be evaluated. This is particularly important because we use time-variant phase shifters, which can also introduce additional sidebands, more importantly, we want to make sure the BPF can eliminate the nonlinearity effects sourced by DAC

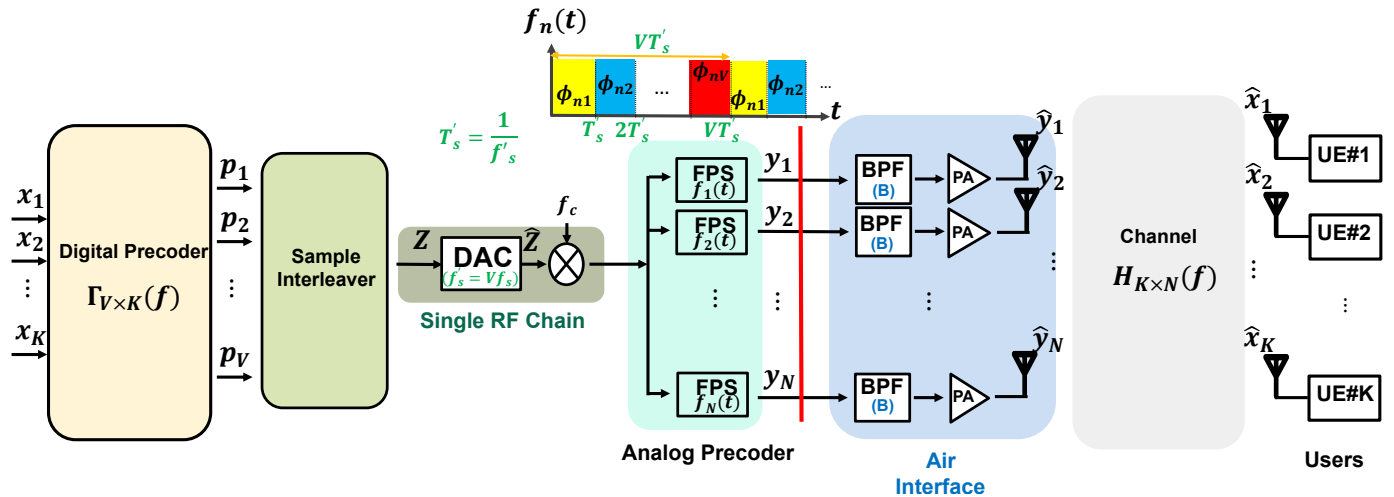


Fig. 3: Architecture of the PhaseMO system, including: 1) Baseband Digital Precoder: The  $V \times K$  matrix  $\Gamma_{V \times K}(f)$  performs digital precoding on users' data vector  $X_{K \times 1}$  with bandwidth B; 2) Interleaver: Organizes the V digitally precoded symbols into a sequence for processing; 3) RF Chain: Interleaved digital samples Z pass through a single RF chain with a DAC (sampling frequency  $f_s$ ) and upconverter to passband  $f_c$ , resulting in analog signals  $\hat{Z}$ ; 4) RF Analog Beamformer: One fast phase shifter (FPS) per antenna generates a time-variant signal  $f_n(t)$ , forming the matrix  $\Phi_{N \times K}$ , mapping the RF chain's analog signals to N output signals  $Y_{N \times 1}$ ; 5) Air Interface Part: Power amplifiers (PAs), antennas, and a bandpass filter clean the spectrum, processing  $Y_{N \times 1}$  to produce  $\hat{Y}_{N \times 1}$ .

non-ideality (i.e. function A) and FPSs. As later on, we have to consider the effect of a bandpass filter on the radiated signal, it is more convenient to do the mathematical analysis of this part in the frequency domain.

We already showed the frequency representation of the DAC output in Eq. 3.To add the DAC non-idealities to this expression, we can write the DAC output spectrum considering function A which models the non-idealities coming from the DAC as  $\hat{Z}(f) = A(Z(f))$  which  $\hat{Z}(f)$  is the DAC output signal in the frequency domain.

In the next step, we will consider the FPS effect on the DAC output and observe how the spectrum is affected by the high-speed switching property of FPS. First, we express the time-domain signal at the output of the FPS and derive its frequency-domain representation as  $y_n(t) = \hat{z}(t) \times f_n(t) \xrightarrow{\mathscr{F}} Y_n(f) = \hat{Z}(f) * F_n(f)$  which  $f_n(t)$  is the time-domain signal created by the FPS. As mentioned previously, each FPS toggles periodically between V phases each of which with  $\frac{1}{Vf_s}$  duration; therefore, we can write down the FPS signal for the nth antenna in one period as follows:

$$f_n(t) = \sum_{v=0}^{V-1} e^{j\Phi_{nv}} \Pi_{T'_s} (t - vT'_s - \frac{T'_s}{2})$$
 (7)

Which  $f_n(t)$  is the time-variant signal produced by the FPS at the n-th antenna,  $\Phi_{nv}$  is the v-th phase produced by the n-th antenna FPS, and  $\Pi_{T_s'}$  demonstrates a pulse with width of  $T_s'$ . Here,  $VT_s'$  is one-period duration, and  $f_s' = Vf_s$  is the DAC sampling frequency of PhaseMO with respect to conventional beamforming sampling frequency( $f_s$ ).

Next, we can extend the Eq. 7 to account for the periodic nature of FPSs. In this regard, we can model the signal using the convolution of a single period with an impulse train which makes the further analysis of the process in the frequency domain easier.

$$f_n(t) = \sum_{i=-\infty}^{\infty} \sum_{v=0}^{V-1} e^{j\Phi_{nv}} \Pi_{T'_s} (t - iVT'_s - vT'_s - \frac{T'_s}{2})$$

$$= \sum_{v=0}^{V-1} e^{j\Phi_{nv}} \sum_{i=-\infty}^{\infty} \left( \Pi_{T'_s} (t - vT'_s - \frac{T'_s}{2}) * \delta(t - iVT'_s) \right)$$
(8)

Finallly, the frequency-domain representation of  $f_n(t)$  can then be derived as:

$$\begin{split} F_{n}(f) &= \sum_{v=0}^{V-1} e^{j\Phi_{nv}} \sum_{i=-\infty}^{\infty} \mathscr{F} \left[ \delta(t-iVT'_{s}) \right] \mathscr{F} \left[ \Pi_{T_{s}}(t-vT'_{s}-\frac{T'_{s}}{2}) \right] \\ &= \sum_{v=0}^{V-1} e^{j\Phi_{nv}} \sum_{i=-\infty}^{\infty} \frac{1}{VT'_{s}} \delta \left( f - \frac{i}{VT'_{s}} \right) T'_{s} e^{-j2\pi f(vT'_{s}+\frac{T'_{s}}{2})} \mathrm{sinc}(fT'_{s}) \\ &= \sum_{v=0}^{V-1} \frac{1}{V} e^{j\Phi_{nv}} \sum_{i=-\infty}^{\infty} \delta \left( f - \frac{i}{VT'_{s}} \right) e^{-j\frac{2\pi i}{VT'_{s}}(vT'_{s}+\frac{T'_{s}}{2})} \mathrm{sinc} \left( \frac{i}{V} \right) \end{split}$$

Substituting  $\hat{Z}(f)$  and  $F_n(f)$  into the  $Y_n(f)=\hat{Z}(f)*F_n(f)$  expression results in:

$$Y_n(f) = \sum_{v=0}^{V-1} \frac{1}{V} e^{j\Phi_{nv}}$$

$$\times \sum_{i=-\infty}^{\infty} A(Z(f)) \Big|_{f=f-\frac{i}{VT_s'}}$$

$$\times e^{-j\frac{2\pi i}{VT_s'}} \operatorname{sinc}\left(\frac{i}{V}\right) \quad (10)$$

This expression indicates that the radiated signal's spectrum, which will be passed through the bandpass filter, includes the DAC's output spectrum and a  $\frac{i}{T_c'V}$  shifted versions of that, resulting from the time-variant phase shifters effect. The bandpass filter will remove all the sidebands out of B bandwidth centered at  $f_c$ , so we need to determine the exact output of the filter.

Simplifying the result, we can observe that the DAC image

artifacts are located at  $if'_s$  frequencies. For values of i that are multiples of V ( $i=\ldots,-2V,-V,0,V,2V,\ldots$ ), the images will be shifted into the pass band of the filter. On the other hand, for these values of i, the Sinc function is only nonzero at i!=0 where we have  $A(Z(f))\approx Z(f)$ . Consequently, the output of the bandpass filter shows that the FPS switching combined with DAC non-idealities can be eliminated using the bandpass filter shown in Eq. 4 and used to prove the adaptability feature of PhaseMO.

#### V. EVALUATION

So far, we have explained the design of the new beamforming architecture, PhaseMO, its operation, and its mathematical representation. In this section, we will discuss various simulation experiments conducted in the downlink scenario assuming perfect channel estimation feedback from the user side to verify PhaseMO's design and demonstrate its key application: load-adaptable power consumption while maintaining good throughput. First, we will describe the evaluation setting. Then, we will compare PhaseMO's throughput with various baselines, including digital beamforming (DBF), fully connected hybrid beamforming (HBF), partially connected hybrid beamforming, analog beamforming (ABF), and GreenMO [31]. We will also examine how PhaseMO achieves reasonable energy efficiency by adapting to network traffic while maintaining coverage area and UE transmit power consumption. Additionally, we will compare PhaseMO's adaptability with antenna muting combined with digital beamforming as the baseline.

#### 1) Evaluation setting

To evaluate PhaseMO, we utilize the frequency channel derived from Sionna, a GPU-accelerated open-source library for link-level simulations based on TensorFlow. Sionna generates the wideband channel frequency response in an open environment model that includes buildings of various sizes. In this study, we set up a base station at a height of 35 meters, equipped with 64 antennas, operating at 4.2 GHz, and consider the distribution of single-antenna users at varying distances from the base station in the provided Munich city map. Specifically, we place one user randomly at a certain distance d from the base station, ensuring that the remaining users are located within a distance less than d. Sionna identifies all beams that can reach the users from the base station and determines the channel impulse response, which includes multiple taps with different phases and attenuations. Finally, it obtains the channel information for each subcarrier based on parameters such as the center frequency (4.2 GHz), number of subcarriers (64), and subcarrier spacing. This configuration is repeated 10 times for each d, as shown in Fig. 4 for the case of 4 users. The evaluation setup, as illustrated in Fig. 4, allows us to comprehensively evaluate PhaseMO in a realistic over-the-air wireless channel scenario.

As shown in Fig. 4, we use Sionna channel frequency response in the MATLAB simulation platform to implement different beamforming techniques. Initially, the random users' bits shaped in 64-QAM constellation points are precoded digitally in orthogonal frequency division multiplexing (OFDM)

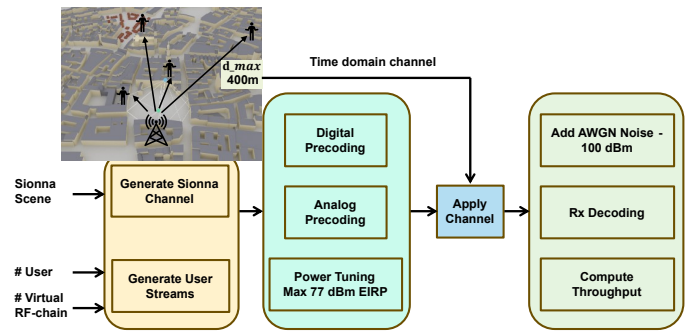


Fig. 4: Evaluation setup using Sionna channel in MATLAB: Users' data is precoded into OFDM symbols (100 MHz), passed through phase shifters, amplified, and transmitted. SINR at users is converted to spectral efficiency and throughput via the 5G-NR MCS table

symbols, each with a 100 MHz bandwidth. Then, the OFDM symbols, after conversion to the time domain, pass through the analog phase-shifter network (i.e., analog or hybrid beamforming). Finally, the filtered radiated signal from each antenna is amplified for over-the-air transmission conditioned not violating maxEIRP of 77dBm limit [35].

On the user side, additive white Gaussian noise (AWGN) with -100 dBm power is added to the received signals. The Error Vector Magnitude (EVM) of the received 64-QAM constellation is computed to derive the user's Signal to Interference + Noise Ratio (SINR) [36]. The SINR is then mapped to spectral efficiency and net throughput using the 5G-NR modulation and coding scheme (MCS) table [37].

## 2) Throughput evaluation

Here, we evaluate PhaseMO in terms of net throughput alongside other beamforming techniques, including DBF, fully connected HBF, partially connected HBF, ABF, and GreenMO. As discussed earlier, to calculate the spectral efficiency (SE) in bps/Hz for each user, we use the 5G-NR MCS table to convert SINR to SE for each user. We then sum the spectral efficiency of all users and consider the total bandwidth used to obtain the net throughput of the system. This process is repeated for different distances from the base station and is averaged over 10 different user configurations.

For each beamforming technique, the corresponding approach is applied. For all beamforming methods, we use the same Zero Forcing (ZF) equalization for digital precoding based on the channel per subcarrier derived from Sionna, while considering the impact of analog precoding. However, we do not utilize intelligent techniques in the analog precoder and use ad-hoc approaches for all methods. For example in GreenMO, since we do not have the BABF approach used in the original design, we instead use a random invertible precoding binary matrix, which is supposed to achieve performance relatively close to the original work. For ABF, hybrid beamforming, and PhaseMO, we employ the center subcarrier channel phase as the analog beamforming approach. For partially connected HBF, we use a combination of the ABF and PhaseMO approaches to generate the analog beamformer design. This ensures a consistent setup for comparisons across all tested methods.

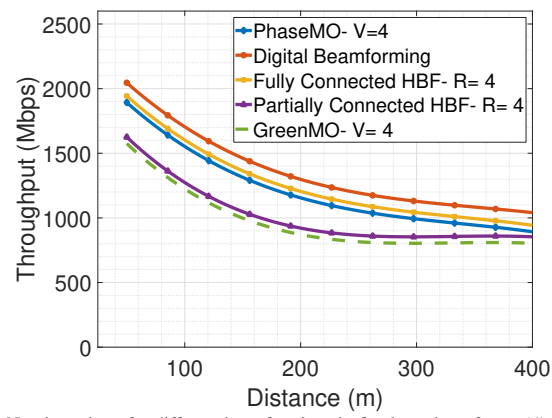


Fig. 5: Net throughput for different beamformings in fixed number of users(4) network, which shows PhaseMO can achieve FCHBF throughout. Figure includes the curves for different beamformings considering 64 antennas and physical or virtual RF chains (V < N) which shows that FCHB and PhaseMO with relatively similar throughput have poorer performance compared to DBF.

In Fig. 5, PhaseMO's net throughput which employs V=4 virtual RF chains with 64 antennas compared to other baselines for 4 users is shown. It is worth noting that, we considered 4 physical RF chains for hybrid beamforming methods in this evaluation. It can be observed that the PhaseMO net throughput is a little bit lower than fully-connected HBF, also it can be observed that partially connected HBF and GreenMO with approximately the same throughput stand below PhaseMO as mentioned previously in [31]. Due to the more strict requirement of using filters in PhaseMO, we account for SINR degradation due to bandpass filter insertion loss considering the 40-45 dB adjacent channel power ratio (ACPR) attenuation for C-band communications [35].

## 3) Adaptability evaluation

To evaluate the adaptability feature of PhaseMO, we analyze throughput degradation and operational power decrease while reducing the number of virtual RF chains. On the other hand, we evaluate the same metrics while using antenna muting combined with digital beamforming (AM +DBF). Finally, combining the power and throughput evaluation, we show how reducing the number of physical RF chains in AM +DBF or virtual RF chains in PhaseMO will affect the energy efficiency (EE) in different load scenarios. In addition, we show how coverage area and UE transmit power will be affected in AM + DBF.

Figure 6.a) shows the power consumption of a traditional 64-antenna BS for varying numbers of active/virtual RF chains. For a base station, the total power consumption is mostly dominated by PAs and base-band processing power consumption. PA power consumption can be calculated based on the number of active RF chains, PA's output power which is defined based on the max EIRP limit, and PA's efficiency. Here, we consider 60% power efficient PAs ([38]) and put the output power of each PA based on maxEIRP of 77dBm. On the other hand, base-band processing power consumption can be evaluated using [39] and [40]. We consider 15GFLOPS for each number of active/virtual RF chains each of which requires 1.683W. So, we can compute the BS power consumption

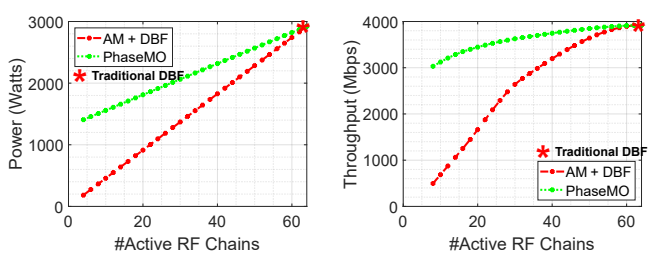


Fig. 6: a) Power consumption, and b) Throughput of antenna muting combined with digital beamforming and PhaseMO versus different numbers of unmuted/virtual RF chains for 8 users is depicted which shows PhaseMO can maintain a good throughput while reducing the power; however, AM+DBF reduces more power at the cost of throughput reduction by a lot

taking into account the power consumption of PAs' and baseband processing.

Although PhaseMO can save about 5-7% power compared to full-capability DBF (all antennas are active), we get more power efficiency comparing its adaptability property with AM+DBF. Taking advantage of AM+DBF to mitigate the power consumption, as we reduce the number of active physical RF chains, both PA power consumption and base-band processing power will drop; however, due to reducing the number of active PAs in the architecture, and multiplexing gain, the system's net throughput will be reduced as well (Fig. 6.b). On the other hand, in PhaseMO similar to hybrid beamforming, if we reduce the number of virtual RF chains, we gain only from reducing the base-band processing power consumption while maintaining all the PAs active which won't cause any throughput reduction.

Therefore, we can evaluate which technique works better in terms of saving power while keeping a reasonable throughput, thus we use energy efficiency  $(\frac{b}{J})$  which combines both of these parameters. As shown in Fig. 7.a) for a network with 8 number of users, using PhaseMO with constant 8 virtual RF chains maintain an energy efficiency higher than the optimum operation point of AM+DBF which is when half of the BS RF chains (32 out of 64) are muted, Consequently, as shown this result in Fig. 7.b) for different number of users, as we increase the number of users up to 8 which is typical number of users connected to today's Massive MIMO BSs, due to less throughput gain of PhaseMO with respect to AM+DBF, the EE improvement gain for PhaseMO in comparison with the best operating point for AM+DBF will reduce to 5% which still is promising.

Although 5% does not look like a promising improvement if we replace AM+DBF with PhaseMO for a case of 8 users, PhaseMO can be considered a better adaptive solution if we include other performance metrics such as coverage area and UE transmit power in uplink. As shown in Fig. 6.b), AM+DBF loses more throughput while trying to achieve a low power consumption due to turning off a few of the antennas and reducing the multiplexity gain. Therefore, it also reduces the coverage area on one side, and on the other side, it makes UE devices draw more power to achieve the same throughput in uplink; however, since PhaseMO just loses some throughput due to less number of virtual RF chains, it won't affect the coverage area and UE transmit power.

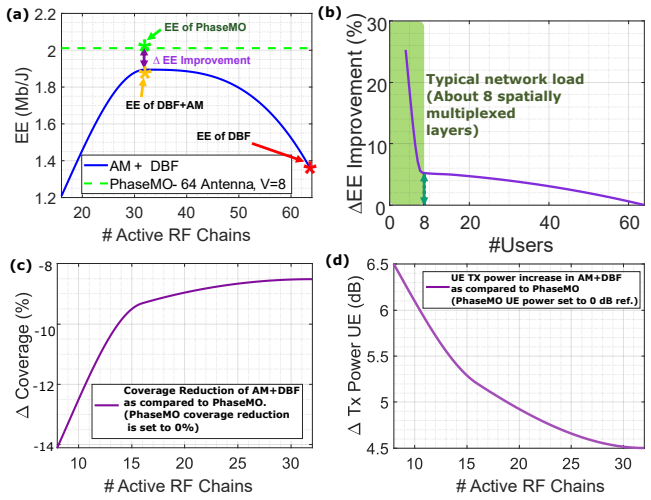


Fig. 7: a) PhaseMO shows better energy efficiency (EE) assuming an equal number of users and virtual RF chains, even when DBF is optimized using AM for 8 users, b) PhaseMO can achieve at least 5% EE improvement for up to 8 users with respect to AM+DBF best point of operation, c) AM+DBF will lose at least 8% coverage area by timing off the half number of RF chains due to less number of active PAs comparing to 64 RF chains full capacity point of operation, d) AM+DBF will cause at least 5dB power increase in UE transmit power consumption due to losing multiplexing gain by reducing half of the BS antennas comparing to 64 RF chains full capacity point of operation

As shown in Fig. 6.c), if we consider the base-station (BS) coverage map with 64 antennas as the baseline in Sionna, due to reducing the number of RF chains the coverage area will decrease and it even reaches about 14% coverage reduction. Additionally, considering the same baseline if we randomly distribute users in the base-station coverage area, the average transmit power of the user will increase by 4.5dB in the best case and 6.5dB in the worst case. As a result, PhaseMO guarantees the worst-case coverage and throughput requirements while improving the energy efficiency of the network. This is achieved by designing an architecture that always uses a maximum number of antennas while flexibly cutting down on digital processing power.

## VI. DISCUSSION AND LIMITATIONS

In this section, we examine the implications of the PhaseMO architecture, acknowledging its limitations and providing insights for future research and potential enhancements.

• Scaling to Higher Number of Antennas: While PhaseMO leverages a single RF chain, scaling beyond 64 antennas is hindered by hardware and design limitations, including the high DAC sampling frequency requirement, phase shifter bandwidth, and power spreading effects. The maximum available DAC sampling frequency today is 6.4 Gsps [41], which supports up to 64 antennas with 100 MHz over-the-air bandwidth. Similarly, the FPS modulation bandwidth, currently limited to 2.5 GHz [8], restricts interfacing to 24 antennas using the current circuit design. Moreover, FPS-induced power spreading attenuates the main band signal's power by  $\frac{1}{V^2}$ , requiring small pre-amplifiers combined with a larger PA providing 47 dB gain. Under these conditions, supporting more than 128 users becomes challenging. To overcome these limitations, a hybrid architecture that combines PhaseMO

- with sets of antennas, each supported by a separate RF chain, can be adapted to enable scalability to higher numbers of antennas.
- Handling Out-of-Band Emission: Due to the spectral spreading effect of FPSs, high-precision narrow-band (100 MHz) bandpass filters with high out-of-band attenuation are necessary to reduce ACPR. However, the non-ideal characteristics of these filters can worsen interference. A potential solution is to use a higher sampling frequency instead of  $V \times$  the signal bandwidth, which simplifies the filtering process and mitigates this limitation.
- Channel Estimation compliance with PhaseMO: The 5G standard for MIMO-based channel estimation at present assumes one antenna mapped to one digital port for channel estimation, which makes it difficult to integrate architectures like PhaseMO, and as well hybrid beamformers. However, there are new changes proposed in release 18 and beyond [42], like orthogonal cover codes can enable more antenna channels from fewer ports, which can make PhaseMO compliant with 5G.
- Comparison Scope and Power-Saving Techniques:
  This work focuses on throughput comparisons with a few selected methods and evaluates power-saving techniques primarily against antenna muting. Furthermore, the precoding techniques used in this study are not chosen optimally. Extending the comparisons to include approaches such as power backoff, other advanced power-efficient methods, and intelligent precoding schemes would provide a more comprehensive analysis and further validate the architecture's performance.

# VII. CONCLUSION

This work introduces PhaseMO, a novel Massive MIMO architecture that dynamically optimizes power consumption based on network load without compromising key performance metrics such as coverage, throughput, and user-device power. By leveraging Fast Phase Shifters (FPS), PhaseMO ensures full array beamforming gain while minimizing digital interfacing in line with network load conditions. Our results demonstrate that PhaseMO achieves an energy efficiency improvement of up to 30 % in low-load scenarios while avoiding approximately 10 % coverage reduction and a 5 dB increase in UE transmit power. Additionally, PhaseMO addresses critical limitations of existing approaches, such as antenna muting and hybrid beamforming, by overcoming hardware scalability challenges and ensuring adaptability to rapidly evolving network demands. These advancements position PhaseMO as a practical and scalable solution for achieving energy-efficient and high-performance cellular networks in the era of increasing connectivity needs.

#### ACKNOWLEDGMENT

This work was supported in part by the U.S. National Science Foundation (NSF) under Award No. 2211805. Further, the authors acknowledge the anonynmous reviewers and WCSNG group members for their feedback.

#### REFERENCES

- S. Networks, Whitepaper: Samsung delivers the promises of massive mimo. [Online]. Available: https://images.samsung.com/is/content/samsung/assets/global/business/networks/insights/white-paper/samsung-delivers-the-promises-of-massive-mimo.ydf.
- [2] M. Yang, Y. Li, D. Jin, L. Su, S. Ma, and L. Zeng, "Openran: A software-defined ran architecture via virtualization," ACM SIGCOMM computer communication review, vol. 43, no. 4, pp. 549–550, 2013.
- [3] X. Costa-Pérez, J. Swetina, T. Guo, R. Mahindra, and S. Rangarajan, "Radio access network virtualization for future mobile carrier networks," *IEEE Communications Magazine*, vol. 51, no. 7, pp. 27–35, 2013.
   [4] P. Rost, I. Berberana, A. Maeder, *et al.*, "Benefits and challenges of virtualiza-
- [4] P. Rost, I. Berberana, A. Maeder, et al., "Benefits and challenges of virtualization in 5g radio access networks," *IEEE Communications Magazine*, vol. 53, no. 12, pp. 75–82, 2015.
- [5] P. Frenger and K. W. Helmersson, "Massive mimo muting using dual-polarized and array-size invariant beamforming," in 2021 IEEE 93rd Vehicular Technology Conference (VTC2021-Spring), IEEE, 2021, pp. 1–6.
- [6] R. Méndez-Rial, C. Rusu, N. González-Prelcic, A. Alkhateeb, and R. W. Heath, "Hybrid mimo architectures for millimeter wave communications: Phase shifters or switches?" *IEEE access*, vol. 4, pp. 247–267, 2016.
- [7] 3gpp study on network energy saving, https://portal.3gpp.org/desktopmodules/ Specifications/SpecificationDetails.aspx?specificationId=3987.
- [8] A. D. Inc., Eval01-hmc877lc3 evaluation board, Accessed: 2024-07-31, 2024.
   [Online]. Available: https://www.digikey.be/en/products/detail/analog-devices-inc/EVAL01-HMC877LC3/3881954.
- [9] S. Han, S. Bian, et al., "Energy-efficient 5g for a greener future," Nature Electronics, vol. 3, no. 4, pp. 182–184, 2020.
- [10] E. Björnson and E. G. Larsson, "How energy-efficient can a wireless communication system become?" In 2018 52nd Asilomar conference on signals, systems, and computers, IEEE, 2018, pp. 1252–1256.
- [11] K. Wang, W. Zhou, and S. Mao, "Energy efficient joint resource scheduling for delay-aware traffic in cloud-ran," in 2016 IEEE Global Communications Conference (GLOBECOM), IEEE, 2016, pp. 1–6.
- [12] L. Kundu, X. Lin, and R. Gadiyar, "Towards energy efficient ran: From industry standards to trending practice," arXiv preprint arXiv:2402.11993, 2024.
- [13] S. Choi, S. Choi, G. Lee, S.-G. Yoon, and S. Bahk, "Deep reinforcement learning for scalable dynamic bandwidth allocation in ran slicing with highly mobile users," *IEEE Transactions on Vehicular Technology*, 2023.
- [14] Y. Azimi, S. Yousefi, H. Kalbkhani, and T. Kunz, "Energy-efficient deep reinforcement learning assisted resource allocation for 5g-ran slicing," *IEEE Transactions on Vehicular Technology*, vol. 71, no. 1, pp. 856–871, 2021.
- [15] S. Wesemann, J. Du, and H. Viswanathan, "Energy efficient extreme mimo: Design goals and directions," *IEEE Communications Magazine*, 2023.
- [16] D. López-Pérez, A. De Domenico, N. Piovesan, et al., "A survey on 5g radio access network energy efficiency: Massive mimo, lean carrier design, sleep modes, and machine learning," *IEEE Communications Surveys & Tutorials*, vol. 24, no. 1, pp. 653–697, 2022.
- [17] R. Guruprasad and S. Dey, "User qos-aware adaptive rf chain switching for power efficient cooperative base stations," *IEEE Transactions on Green Communications and Networking*, vol. 1, no. 4, pp. 409–422, 2017.
- [18] J. Akhtar, K. Rajawat, V. Gupta, and A. K. Chaturvedi, "Joint user and antenna selection in massive-mimo systems with qos-constraints," *IEEE Systems Journal*, vol. 15, no. 1, pp. 497–508, 2020.
- [19] S. Bassoy, R. Behravesh, and J. Pujol-Roig, "Seedrl: Smart energy efficiency using deep reinforcement learning for 6g networks," in 2023 IEEE Globecom Workshops (GC Wkshps), IEEE, 2023, pp. 732–737.
- [20] N. Rajapaksha, J. Mohammadi, S. Wesemann, T. Wild, and N. Rajatheva, "Minimizing energy consumption in mu-mimo via antenna muting by neural networks with asymmetric loss," *IEEE Transactions on Vehicular Technology*, 2023
- [21] F. H. Ahmadzai and W. Lee, "Adaptive antenna muting using rnn-based traffic load prediction," *Journal of the Korea Institute of Information and Communication Engineering*, vol. 26, no. 4, pp. 633–636, 2022.
- [22] T. Kühne, P. Gawłowicz, A. Zubow, F. Dressler, and G. Caire, "Bringing hybrid analog-digital beamforming to commercial MU-MIMO wifi networks," in Proceedings of the 26th Annual International Conference on Mobile Computing and Networking, 2020, pp. 1–3.
- [23] S. Mondal, R. Singh, and J. Paramesh, "21.3 a reconfigurable bidirectional 28/37/39GHz front-end supporting MIMO-TDD, carrier aggregation TDD and FDD/Full-duplex with self-interference cancellation in digital and fully connected hybrid beamformers," in 2019 IEEE International Solid-State Circuits Conference-(ISSCC), IEEE, 2019, pp. 348–350.
- [24] S. Mondal, R. Singh, A. I. Hussein, and J. Paramesh, "A 25–30 GHz fully-connected hybrid beamforming receiver for MIMO communication," *IEEE Journal of Solid-State Circuits*, vol. 53, no. 5, pp. 1275–1287, 2018.
- Journal of Solid-State Circuits, vol. 53, no. 5, pp. 1275–1287, 2018.

  [25] H.-T. Kim, B.-S. Park, S.-S. Song, et al., "A 28-GHz cmos direct conversion transceiver with packaged 2\*4 antenna array for 5G cellular system," IEEE Journal of Solid-State Circuits, vol. 53, no. 5, pp. 1245–1259, 2018.
- [26] X. Xie, E. Chai, X. Zhang, K. Sundaresan, A. Khojastepour, and S. Rangarajan, "Hekaton: Efficient and practical large-scale MIMO," in *Proceedings of the 21st Annual International Conference on Mobile Computing and Networking*, 2015, pp. 304–316.

- [27] Y. Chen, Y. Huang, C. Li, Y. T. Hou, and W. Lou, "Turbo-HB: A novel design and implementation to achieve ultra-fast hybrid beamforming," in *IEEE INFOCOM 2020-IEEE Conference on Computer Communications*, IEEE, 2020, pp. 1489–1498.
- [28] X. Yu, J.-C. Shen, J. Zhang, and K. B. Letaief, "Alternating minimization algorithms for hybrid precoding in millimeter wave MIMO systems," *IEEE Journal of Selected Topics in Signal Processing*, vol. 10, no. 3, pp. 485–500, 2016.
- [29] H. Yan, S. Ramesh, T. Gallagher, C. Ling, and D. Cabric, "Performance, power, and area design trade-offs in millimeter-wave transmitter beamforming architectures," *IEEE Circuits and Systems Magazine*, vol. 19, no. 2, pp. 33–58, 2019
- [30] C. N. Barati, S. Dutta, S. Rangan, and A. Sabharwal, "Energy and latency of beamforming architectures for initial access in mmwave wireless networks," *Journal of the Indian Institute of Science*, vol. 100, no. 2, pp. 281–302, 2020.
- [31] A. Gupta, S. Nassirpour, M. Dunna, E. Patamasing, A. Vahid, and D. Bharadia, "Greenmo: Enabling virtualized, sustainable massive mimo with a single rf chain," in *Proceedings of the 29th Annual International Conference on Mobile Computing and Networking*, 2023, pp. 1–17.
- [32] G. Bogdan, K. Godziszewski, and Y. Yashchyshyn, "Time-modulated antenna array for real-time adaptation in wideband wireless systems-part ii: Adaptation study," *IEEE Transactions on Antennas and Propagation*, vol. 68, no. 10, pp. 6973–6981, 2020.
- [33] J. P. González-Coma and L. Castedo, "Wideband hybrid precoding using time modulated arrays," *IEEE Access*, vol. 8, pp. 144638–144653, 2020.
- [34] P. M. I. (PMI), Ps-360-6g18g-5-sff digital phase shifter, https://www.everythingrf.com/products/digital-phase-shifters/planar-monolithics-industries/627-80-ps-360-6g18g-5-sff, Accessed: YYYY-MM-DD.
- [35] N. Telecommunications and I. Administration, Tr-22-562: Assessment of 5g security challenges, Accessed: 2023-10-22, 2022. [Online]. Available: https://its.ntia.gov/publications/download/TR-22-562.pdf.
- [36] T. W. Brown, D. A. Humphreys, M. Hudlicka, and T. H. Loh, "Prediction of sinr using ber and evm for massive mimo applications," in 12th European Conference on Antennas and Propagation (EuCAP 2018), IET, 2018, pp. 1–5.
- [37] A. K. Thyagarajan, P. Balasubramanian, D. Vydeki, and M. Karthik, "Snr-cqi mapping for 5g downlink network," in 2021 IEEE Asia Pacific Conference on Wireless and Mobile (APWiMob), IEEE, 2021, pp. 173–177.
- [38] K. Kim, T. Lee, and M. Kim, "High efficiency power amplifiers for rf and microwave applications," *IEEE Transactions on Microwave Theory and Techniques*, vol. 68, no. 10, pp. 3220–3230, Oct. 2020. DOI: 10.1109/TMTT. 2020.2992054.
- [39] L. M. M. Zorello, M. Sodano, S. Troia, and G. Maier, "Power-efficient baseband-function placement in latency-constrained 5g metro access," *IEEE Transactions on Green Communications and Networking*, vol. 6, no. 3, pp. 1683–1696, 2022.
- [40] E. Björnson, E. G. Larsson, and T. L. Marzetta, "Massive mimo: Ten myths and one critical question," *IEEE Communications Magazine*, vol. 54, no. 2, pp. 114–123, 2016.
- [41] A. Devices, Ad9162: Dual-channel, 16-bit, 6.4 gsps dac with high-speed digital interface, Accessed: 2024-07-31, 2024. [Online]. Available: https://www.analog. com/en/products/ad9162.html.
- [42] H. Jin, K. Liu, M. Zhang, et al., "Massive mimo evolution toward 3gpp release 18," IEEE Journal on Selected Areas in Communications, vol. 41, no. 6, pp. 1635–1654, 2023.